Spray Coating Experiments: Setups and Methodologies

The latest eBook from Advanced Optical Metrology. Download for free.

Spray Coating Experiments: Setups and Methodologies, is the third in our Thin Films eBook series. This publication provides an introduction to spray coating, three article digests from Wiley Online Library and the latest news about Evident's Image of the Year Award 2022.

Wiley in collaboration with Evident, are committed to bridging the gap between fundamental research and industrial applications in the field of optical metrology. We strive to do this by collecting and organizing existing information, making it more accessible and useful for researchers and practitioners alike.

EVIDENT
OLYMPUS

WILEY

NANO · MICRO small
www.small-journal.com

Synthesis of Thermally Stable and Highly Luminescent $Cs_5Cu_3Cl_6I_2$ Nanocrystals with Nonlinear Optical Response

*Changhee Jang, Kangyong Kim, Hak-Won Nho, Seung Min Lee, Hanif Mubarok, Joo Hyeong Han, Hyeonjung Kim, Dongryeol Lee, Yangpil Jang, Min Hyung Lee, Oh-Hoon Kwon, Sang Kyu Kwak, Won Bin Im, Myoung Hoon Song, and Jongnam Park**

Low-dimensional Cu(I)-based metal halide materials are gaining attention due to their low toxicity, high stability and unique luminescence mechanism, which is mediated by self-trapped excitons (STEs). Among them, $Cs_5Cu_3Cl_6I_2$, which emits blue light, is a promising candidate for applications as a next-generation blue-emitting material. In this article, an optimized colloidal process to synthesize uniform $Cs_5Cu_3Cl_6I_2$ nanocrystals (NCs) with a superior quantum yield (QY) is proposed. In addition, precise control of the synthesis parameters, enabling anisotropic growth and emission wavelength shifting is demonstrated. The synthesized $Cs_5Cu_3Cl_6I_2$ NCs have an excellent photoluminescence (PL) retention rate, even at high temperature, and exhibit high stability over multiple heating–cooling cycles under ambient conditions. Moreover, under 850-nm femtosecond laser irradiation, the NCs exhibit three-photon absorption (3PA)-induced PL, highlighting the possibility of utilizing their nonlinear optical properties. Such thermally stable and highly luminescent $Cs_5Cu_3Cl_6I_2$ NCs with nonlinear optical properties overcome the limitations of conventional blue-emitting nanomaterials. These findings provide insights into the mechanism of the colloidal synthesis of $Cs_5Cu_3Cl_6I_2$ NCs and a foundation for further research.

1. Introduction

Metal halide semiconductors are currently among the most widely studied materials due to their unique optoelectronic properties.[1–11] In particular, remarkable achievements in the field of optoelectronics have been demonstrated using lead halide perovskites, which have the general formula $APbX_3$ (A = $CH_3NH_3^+$, $HC(NH_2)_2^+$, Cs^+; X = Cl^-, Br^-, I^-).[12–21] Despite the great advances reported in $APbX_3$ research over the past decade, the high toxicity of Pb and the intrinsic chemical instability of these materials limit their practical applicability.[22–24] Isovalent substitutes for Pb^{2+}, such as Sn^{2+} or Ge^{2+}, have been considered in the hope of developing lead-free metal halide perovskites; however, these species are easily oxidized to tetravalent ions under ambient conditions and are self-doped within the crystals as

C. Jang, K. Kim, S. M. Lee, H. Kim, J. Park
School of Energy and Chemical Engineering
Ulsan National Institute of Science and Technology (UNIST)
Ulsan 44919, Republic of Korea
E-mail: jnpark@unist.ac.kr

H.-W. Nho, O.-H. Kwon
Department of Chemistry
College of Natural Sciences
Ulsan National Institute of Science and Technology (UNIST)
Ulsan 44919, Republic of Korea

H.-W. Nho, O.-H. Kwon
Center for Soft and Living Matter
Institute for Basic Science (IBS)
Ulsan 44919, Republic of Korea

The ORCID identification number(s) for the author(s) of this article can be found under https://doi.org/10.1002/smll.202206668.

DOI: 10.1002/smll.202206668

H. Mubarok, M. H. Lee
Department of Chemistry
University of Ulsan
Ulsan 44610, Republic of Korea

J. H. Han, W. B. Im
Division of Materials Science and Engineering
Hanyang University
Seoul 04763, Republic of Korea

D. Lee, M. H. Song
Department of Materials Science and Engineering
Ulsan National Institute of Science and Technology (UNIST)
Ulsan 44919, Republic of Korea

Y. Jang, J. Park
Department of Biomedical Engineering
Ulsan National Institute of Science and Technology (UNIST)
Ulsan 44919, Republic of Korea

S. K. Kwak
Department of Chemical and Biological Engineering
Korea University
145 Anam-ro, Seongbuk-gu, Seoul 02841, Republic of Korea

p-type dopants, negatively affecting the photoelectric properties.[25–28] Double perovskites (elpasolites) and Bi,Sb trivalent metal halides have also been proposed, but their photoluminescence (PL) efficiencies are much lower than those of Pb-based halides, and the demand for next-generation metal halide semiconductors with excellent quantum efficiency and stability has increased.[3,29–32]

Recently, Cu-based metal halides have gained popularity due to their low toxicity, high stability, and unique PL process mediated by self-trapped excitons (STEs).[1,33–65] STEs are formed during a process in which excitons are trapped in a local potential minima generated by the distorted lattice upon photoexcitation, typically in soft ionic crystals with strong electron–phonon interactions.[66–70] Since exciton localization is an effective strategy to promote radiative recombination, various methods to achieve this have been reported, such as quantum well formation based on core–shell structures,[71–74] lattice periodicity reduction via doping,[75] and morphological control to enhance the effects of quantum confinement.[76–79] From this perspective, STEs can also be considered as a key approach for the design of semiconductor materials with excellent luminous efficiencies. In 2018, Jun et al. synthesized single-crystal $Cs_3Cu_2I_5$, consisting of spatially isolated [Cu-I] polyhedra, for the first time. An emission band assigned to STEs, which were generated because of the low-dimensionality of the electronic structure, was shown to possess an excellent PL quantum yield (QY) of up to 90%.[33] In addition, $Cs_3Cu_2I_5$ displayed a broad emission band with a large Stokes shift, which are characteristics of STEs that are primarily seen in Cu(I)-based fluorescence. Following the initial $Cs_3Cu_2I_5$ study, analogs such as $CsCu_2X_3$ and $Cs_3Cu_2X_5$ (X = Cl, Br, I) were synthesized, both in the bulk and as nanocrystals (NCs),[34–42] and in-depth analyses of their photophysical properties[43]—as well as studies on various applications, from scintillators to light-emitting diodes[44–46]—were also carried out.

In 2020, Hosono's group reported the first synthesis of the mixed-halide compound $Cs_5Cu_3Cl_6I_2$ as a single crystal with pure-blue emission (≈462 nm).[64] Among the existing blue-emitting quantum dots, there are limited applications for CdSe,[80,81] ZnSeTe[82–85] and $CsPb(Cl,Br)_3$[86–90] quantum dots because of the severe toxicity of Cd, Te and Pb.[91–93] Indium phosphide (InP) has relatively low toxicity, but the bandgap of the bulk material is small (1.35 eV), so reducing the size of particles is essential, and pure-blue-emitting InP quantum dots with high stability and QY must be synthesized.[94–97] Therefore, $Cs_5Cu_3Cl_6I_2$, with low toxicity and excellent QY, has excellent application potential as a next-generation blue-emitting material. However, despite these promising possibilities, $Cs_5Cu_3Cl_6I_2$ has not been subjected to much detailed study owing to the challenges involved in engineering its structure and composition. Recently, Duan et al. reported a study on $Cs_5Cu_3Cl_6I_2$ NCs, but their QY was shown to be relatively low (73.7%) compared to that of the bulk crystal, and they exhibited rapid thermal quenching during heating (270–320 K).[65] In addition, the optical bandgap was reported to be 4.92 eV, which is very large, and only a narrow absorption in the UV region was observed, making it difficult to utilize the optical properties of this material and further limiting its applicability. In this study, we designed an effective colloidal process to synthesize monodisperse $Cs_5Cu_3Cl_6I_2$ NCs with a superior QY (≈100%) and thermal stability. We performed a careful analysis of the effects of the reaction parameters on the anisotropic growth of $Cs_5Cu_3Cl_6I_2$ NCs. Our results identified the tunability of the STE energy level of $Cs_5Cu_3Cl_{8-x}I_x$ that can be achieved via halide engineering, and confirmed the nonlinear optical response of the material, thereby expanding its application scope.

2. Results and Discussion

We synthesized the $Cs_5Cu_3Cl_6I_2$ NCs using the colloidal hot-injection method (**Figure 1**a). The crystal structure of $Cs_5Cu_3Cl_6I_2$ (orthorhombic, *Cmcm* space group) is shown in Figure 1b, where 1D zigzag chains of $[Cu_3Cl_6I_2]_n^{5n-}$ are charge-balanced by Cs^+ cations. These crystal structure characteristics were validated by comparing the X-ray diffraction (XRD) pattern with a reference pattern for $Cs_5Cu_3Cl_6I_2$; the patterns were quite consistent, indicating an absence of impurities in our sample (Figure 1c). The morphology and size dispersity of the $Cs_5Cu_3Cl_6I_2$ NCs was further investigated by transmission electron microscopy (TEM). The TEM analysis results (Figure 1d and Figure S1a, Supporting Information), confirmed that rhombohedron-shaped NCs with an average size of 29.8 nm had been uniformly synthesized. These NCs had high crystallinity and the interplanar spacing (*d* spacing) was found to be 0.336 nm, which is consistent with the (313) *d* spacing in $Cs_5Cu_3Cl_6I_2$. Figure S1b, Supporting Information, shows the $Cs_5Cu_3Cl_6I_2$ NC solution, which exhibits high dispersibility as well as bright pure-blue PL upon it being irradiated with 254-nm UV light (Figure 1e). UV–visible (UV–Vis) absorption and PL spectroscopy were used to examine the optical characteristics of the $Cs_5Cu_3Cl_6I_2$ NCs. The as-synthesized $Cs_5Cu_3Cl_6I_2$ NCs exhibited a sharp absorption peak at 280 nm. Analyzing the PL and QY of the sample revealed that its PL was pure-blue (centered at 464 nm), and that its QY was up to 100% (average: 98.0%, standard deviation: 1.37%). The superior QY is attributed to an increase in the recombination probability, owing to exciton localization and inhibition of reabsorption because of the large Stokes shift of up to 180 nm, which is evidence for the formation of STEs. Furthermore, the full-width at half-maximum (FWHM) of the emission band was reduced by 13% compared to the value for the bulk crystal, because of the high crystallinity and size uniformity of the NCs.

To understand the growth kinetics of the $Cs_5Cu_3Cl_6I_2$ NCs and optimize the colloidal synthesis process, the reaction-time dependence of the growth of the NCs was investigated (**Figure 2**a,b). At the initial stage of the reaction (10 s), particles with irregular shapes and sizes, ranging from nuclei with a size of less than 3 nm to particles with a size of about 20 nm, were observed. These highly ionic crystals grew rapidly and exhibited a bimodal size distribution at 20 s, with large already grown particles and small seeds. This growth behavior was observed because, after the injection of cesium oleate (Cs(OAc)), the monomer was not rapidly consumed below a critical concentration owing to the relatively low reaction temperature (80 °C). As a result, the nucleation and growth stages could not be separated temporally, and the secondary nucleated seeds and the grown particles were observed together at 20 s. However, as

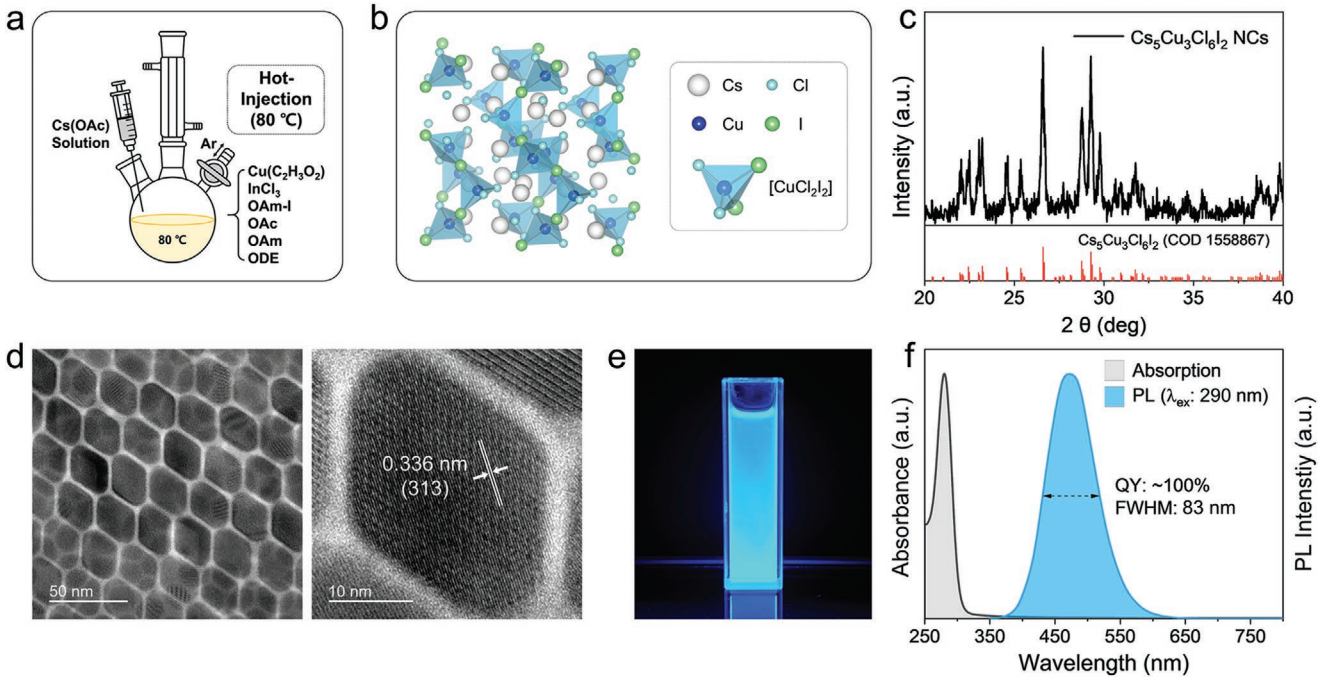

Figure 1. Synthesis and characterization of $Cs_5Cu_3Cl_6I_2$ NCs. a) Schematic illustration of the colloidal synthesis of $Cs_5Cu_3Cl_6I_2$ NCs. b) Schematic view $Cs_5Cu_3Cl_6I_2$ NC crystal structure. c) XRD characterization of $Cs_5Cu_3Cl_6I_2$ NCs: experimental (top) and reference (bottom) spectra. d) TEM images of $Cs_5Cu_3Cl_6I_2$ NCs. e) Photograph of $Cs_5Cu_3Cl_6I_2$ NC solution under 254 nm excitation (solvent: hexane). f) Absorption and PL spectra of $Cs_5Cu_3Cl_6I_2$ NCs.

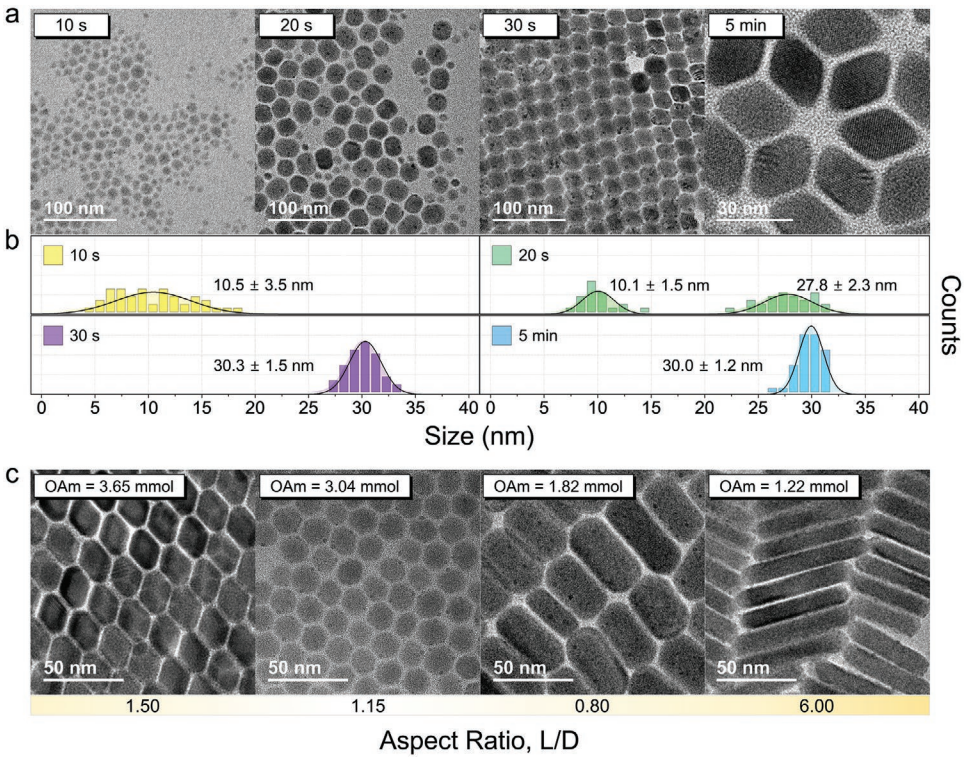

Figure 2. Effects of reaction parameter variation. a) TEM images of $Cs_5Cu_3Cl_6I_2$ NCs synthesized using different growth times; 10 s, 20 s, 30 s, and 5 min, respectively. Particle size is expressed as mean ± standard deviation. b) Size distribution histograms with Gaussian fits of the $Cs_5Cu_3Cl_6I_2$ NCs synthesized using the different growth times. c) TEM images (top) and aspect ratio (length/diameter [*L*/*D*]; bottom) of $Cs_5Cu_3Cl_6I_2$ NCs synthesized using different OAm amounts (3.65, 3.04, 1.82, and 1.22 mmol, respectively).

the reaction continued, particles with a size below the critical radius were dissolved, and size-focusing occurred. Indeed, 30 s after the injection, the particles had converged to a uniform size and shape, indicating that the reaction produced a thermodynamically controlled product at 80 °C. The single absorption peak in Figure S2a,b, Supporting Information, demonstrates that no byproducts were generated, and the slight redshift of the peak can be attributed to an increase in the particle size. Furthermore, temporal evolution of PL spectrum during growth (Figure S2c, Supporting Information) shows a new PL peak around 350–400 nm and a low-energy tail over 550 nm along with the main peak at 464 nm at the initial stage of growth (10 s). A previous study reporting the quantum confinement effect of $Cs_3Cu_2I_5$ quantum dots indicate that the blue-shifted PL (350–400 nm) originates from $Cs_5Cu_3Cl_6I_2$ quantum dots, which are seeds less than 3 nm observed in TEM.[42] As the growth continues, the ratio of quantum dots that appeared temporarily at the beginning of the reaction gradually decreased, and the tail observed over 550 nm gradually diminished by the process of growth and surface stabilization. Finally, the reaction was continued for a further 5 min to obtain monodisperse $Cs_5Cu_3Cl_6I_2$ NCs with high crystallinity. Furthermore, by comparing NCs prepared at different temperatures, it was established that 80 °C was the optimum reaction temperature in terms of the QY, and that this temperature produced a desirable size distribution (Figure S3, Supporting Information). Figure S4, Supporting Information, shows the SEM analysis results for the sample prepared via a reaction at 150 °C (30 min); growth was not constrained to the nanoscale, and rhombohedral particles with sizes of several micrometers were generated.

Previous research results, including on perovskites such as $CsPbX_3$ (X = Cl, Br, I), indicate that anisotropic growth can be induced by careful selection of ligands to synthesize NCs with various morphologies and broad application ranges.[14,15,98–100] Therefore, we attempted to synthesize morphologically controlled $Cs_5Cu_3Cl_6I_2$ NCs via ligand engineering. As the amount of added oleylamine (OAm) was gradually decreased, 1D growth was induced with a gradually increasing aspect ratio (Figure 2c). The particle shapes changed from rhombohedral to hexagonal when the OAm amount decreased from 3.65 to 3.04 mmol, becoming 1D nanorods and growing longer when the OAm amount was decreased to 1.82 and 1.22 mmol. Considering previous studies in which morphological changes were induced by tuning the acid-to-amine ligand ratio,[15,100] it can be inferred that the exposed facet in the growth direction has a high binding affinity for amine. Therefore, in our study, as the amount of the amine was reduced and the probability of ligand dissociation on the facet increased, the adsorption of the monomer became more favorable as a means of lowering the surface energy. Thus, by controlling the synthesis parameters, we were able to gain insights into the growth behavior of the $Cs_5Cu_3Cl_6I_2$ NCs, obtain NCs with a high QY and size uniformity under optimized experimental conditions, and induce anisotropic growth.

We investigated whether the emission wavelength can be controlled via halide engineering, as is the case for Pb-based perovskites whose bandgap can be tuned by adjusting the halide composition. Figure S5, Supporting Information, shows the change in the PL spectrum when the ratio between the amounts of $InCl_3$ and oleylammonium iodide (OAm-I) in the batch was increased from 3:1 to 5:1; specifically, the PL peak was red-shifted from 464 to 478 nm. In addition, in order to increase the Cl doping level, the reaction temperature was increased from 80 to 140 °C. **Figure 3**a shows the PL and PL excitation (PLE) spectra of two samples: one prepared using an $InCl_3$:OAm-I ratio of 3:1 at 80 °C (CCH-1) and the other prepared using an $InCl_3$:OAm-I ratio of 5:1 at 140 °C (CCH-2). The absorption (Figure S6a, Supporting Information) and PLE (Figure 3a) spectra of CCH-1 and CCH-2 were almost identical, but in the case of the PL wavelength, a red-shift was observed from 464 (CCH-1) to 488 nm (CCH-2, QY: 86%). It has been reported that PL peak wavelength changes with halide composition for $Cs_3Cu_2X_5$ (X = Cl, Br, I) structures tend to be the opposite of those observed for Pb-based perovskites.[34,43] The calculated bandgaps of $Cs_3Cu_2X_5$ and $CsPbX_3$ both follow the order Cl > Br > I, but after photoexcitation, the change in the valence band maxima (VBM) owing to local lattice deformation and the difference in exciton binding and self-trapping energies reverses the order of the emission energies (wavelengths).[34] Thus, the observed PL red-shift of CCH-2 can be attributed to the substitution of I in $Cs_5Cu_3Cl_6I_2$ with Cl. Figure S6b, Supporting Information, shows the XRD patterns of CCH-1 and CCH-2. These have the same form, indicating that no new phase was formed, but the CCH-2 pattern is shifted to a slightly higher angle compared to the CCH-1 pattern; the (313) peak was shifted by +0.19° (Figure 3b), which is likely to be the result of lattice contraction when some of the I ions (ionic radius: 206 pm) were replaced by Cl (ionic radius: 181 pm). The effect of increased Cl incorporation was also observed via X-ray photoelectron spectroscopy (XPS). As the amount of highly electronegative Cl increased, the overall electronegativity of the $Cs_5Cu_3Cl_{8-x}I_x$ NCs was altered, and the XPS peaks shifted to higher binding energies (Figure 3c and Figure S7, Supporting Information). Taken together, these observations suggest that the difference between the CCH-1 and CCH-2 PL spectra can be understood as resulting from Cl incorporation, and the quantitative XPS analysis (Figure S7e, Supporting Information) revealed that the amount of Cl in CCH-2 was 8% higher than that in CCH-1. In addition, it should be noted that although $InCl_3$ was used as a Cl source for the synthesis, no In signal was observed in the product. This result is in agreement with the results of a prior study in which ZnX_2, a heterogeneous metal halide, was employed as a halide source in the synthesis of the $CsPbX_3$ perovskite without Zn incorporation.[101] Furthermore, as the weak satellite peak at 945 eV in Figure 3c can be attributed to monovalent Cu, information on the oxidation number of Cu in the NCs was extracted from our XPS analysis.[102]

We used density functional theory (DFT) to determine the relationship between the composition, as revealed by quantitative analysis, and the observed optical properties. Figure S8, Supporting Information, shows the simulated $Cs_5Cu_3Cl_6I_2$ unit cell containing two 1D $[Cu_6Cl_{12}I_4]$ chains; it is apparent that there are eight iodine ions in the unit cell. Note that the crystal structure of $Cs_5Cu_3Cl_6I_2$ was obtained from a previous study.[64] Subsequently, the crystal structure of $Cs_5Cu_3Cl_7I_1$, the composition that can be considered to correspond to CCH-2, was theoretically predicted by introducing four chlorine ions into iodine sites in $Cs_5Cu_3Cl_6I_2$. To compare thermodynamically preferred

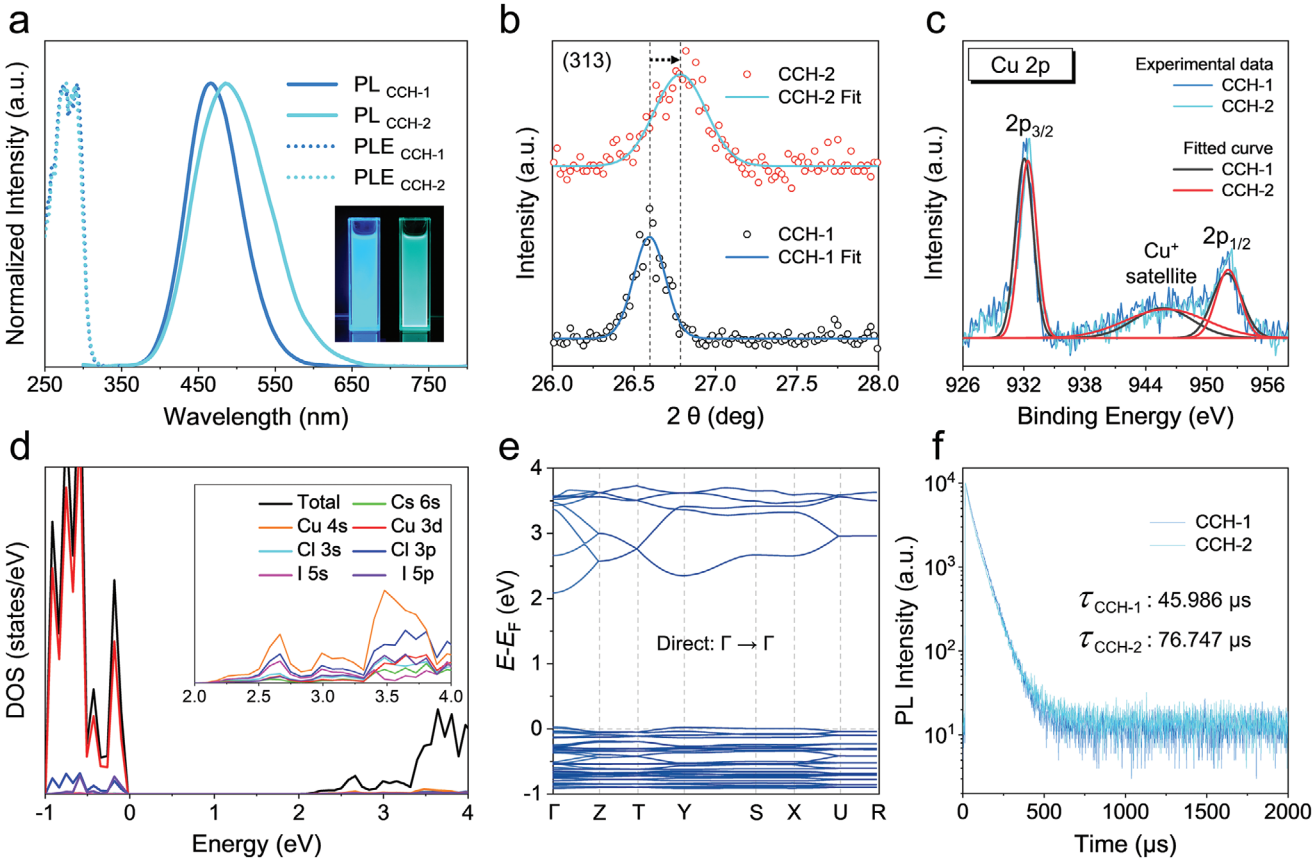

Figure 3. Characterization of two different $Cs_5Cu_3Cl_{8-x}I_x$ NC samples, CCH-1 and CCH-2. a) PL and PLE spectra (inset: photographs of CCH-1 and CCH-2 solutions under 254-nm excitation). b) Expanded XRD patterns. c) Cu 2p XPS spectra of CCH-1 and CCH-2. d) Partial and total DOS. e) Calculated band structure of $Cs_5Cu_3Cl_6I_2$. f) TRPL spectra of CCH-1 and CCH-2.

doping sites, the relative energies of chlorine-doped $Cs_5Cu_3Cl_7I_1$ structures were calculated (Figure S9, Supporting Information). The relative energy result suggests that the $Cs_5Cu_3Cl_7I_1$ structure in which four iodine ions from one $[Cu_6Cl_{12}I_4]$ chain are replaced with chlorine ions (sites 5 to 8) is the most thermodynamically stable. Based on this structural information, we calculated the density of states (DOS) and band structures of $Cs_5Cu_3Cl_6I_2$ (Figure 3d,e) and $Cs_5Cu_3Cl_7I_1$ (Figure S10, Supporting Information). Parameters related to the two calculated crystal structures are presented in Table S1, Supporting Information. In both structures, the valence band maximum (VBM) is formed mainly from the Cu 3d, Cl 3p, and I 5p orbitals. However, in the conduction band minima (CBM), which are mainly derived from Cu 4s and Cl 3p orbitals, the contribution of I 5s was lower for $Cs_5Cu_3Cl_7I_1$ than for $Cs_5Cu_3Cl_6I_2$. Furthermore, unlike $Cs_5Cu_3Cl_6I_2$, which has a direct bandgap, the substituted structure has an indirect bandgap, which is related to the comparatively low QY (≈86%) of CCH-2.

To further investigate the differences between the optical characteristics of CCH-1 and CCH-2, a time-resolved photoluminescence (TRPL) analysis was performed. These Cs—Cu—X materials have decay lifetimes on the order of microseconds because their PL occurs via a STE mechanism. The TRPL analysis results (Figure 3f and Table S2, Supporting Information,) revealed that CCH-1 and CCH-2 exhibited bi- and tri-exponential decay with average lifetimes of 45.986 and 76.747 μs, respectively. The decay lifetimes of $Cs_3Cu_2X_5$ follow the order I < Br < Cl, and therefore the greater lifetime increase for CCH-2 can also be interpreted being a result of the STE mechanism revealed in Cs—Cu—X.

Blue-emitting semiconductors, such as $CsPbBr_3$, have excellent luminescent properties, but have limited application potential because of their inherently low stability. Specifically, they are vulnerable to moisture in the atmosphere and are easily damaged by Joule heating during device operation. Therefore, we performed thermal-stability testing to assess the applicability of the $Cs_5Cu_3Cl_6I_2$ NCs. **Figure 4**a shows a pseudocolor map of the temperature dependence of the PL emission spectrum of a $Cs_5Cu_3Cl_6I_2$ thin film in the range of 298–473 K. An excellent PL retention rate at 473 K of 28%, compared to the PL at room temperature, is apparent, and no changes or shifts in the shape of the spectrum are seen over the temperature range shown. We attempted to verify the superior thermal stability of the $Cs_5Cu_3Cl_6I_2$ NCs, comparing them with quantum-confined $CsPbBr_3$ NCs, which are currently among the most well-known blue-emitting materials. Figure S11, Supporting Information, shows photographs of the PL of $Cs_5Cu_3Cl_6I_2$ thin film in air at 25 and 100 °C, and the PL of $Cs_5Cu_3Cl_6I_2$ was intense even at 100 °C. To determine the origin of the excellent thermal stability of the $Cs_5Cu_3Cl_6I_2$ PL, the exciton binding energy was calculated (Figure 4b). An Arrhenius plot of the integrated PL

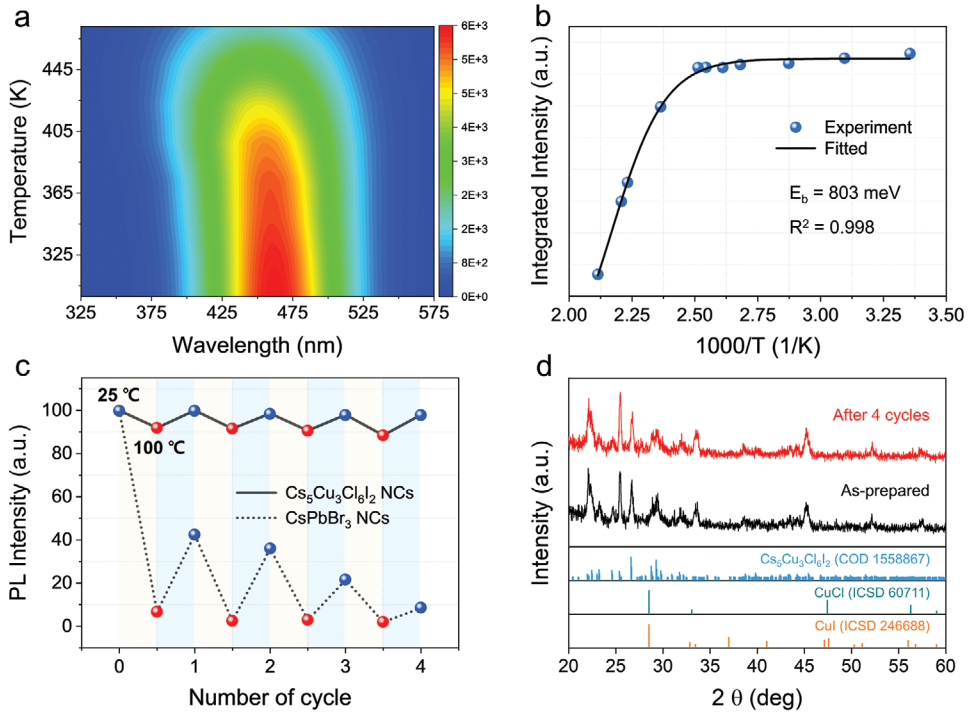

Figure 4. Temperature-dependent $Cs_5Cu_3Cl_6I_2$ NC properties. a) Pseudocolor map showing temperature dependence of PL spectra of $Cs_5Cu_3Cl_6I_2$ NC thin film between 298 and 473 K. b) Integrated PL intensity versus 1000/*T*. c) PL intensity of the $Cs_5Cu_3Cl_6I_2$ (solid line) and $CsPbBr_3$ (dotted line) films during multiple heating (100 °C, red dot) and cooling (25 °C, blue dot) cycles; experiments were carried out in ambient condition, relative humidity: 32%, d) XRD patterns of $Cs_5Cu_3Cl_6I_2$ NCs thin film; as-prepared (black) and after four heating–cooling cycles.

intensity can be used to show the temperature dependence of the nonradiative process, and the exciton binding energy can be calculated using the following equation:

$$I(T) = \frac{I_0}{1 + A\exp\left(-\frac{E_b}{k_B T}\right)} \quad (1)$$

where $I(T)$ and I_0 are the integrated PL intensities at temperatures T and 0 K, respectively, A is the proportionality parameter of the nonradiative process, E_b is the exciton binding energy, and k_B is the Boltzmann constant.[33,103] As a result of fitting, a value of E_b of 803 meV was extracted; this value is much larger than E_b values for blue-emitting nanomaterials such as Pb-based perovskites and ZnSeTe quantum dots.[18,104] This binding energy is high because of the inclusion of self-trapping energy in the low-dimensional electronic structure of $Cs_5Cu_3Cl_6I_2$, which is directly related to its high QY and thermal stability. Moreover, the exciton–phonon coupling behavior in $Cs_5Cu_3Cl_6I_2$ NCs is reflected by the Huang–Rhys factor (S) which can be calculated by fitting the temperature-dependent FWHM using the following equation:[105]

$$\mathrm{FWHM} = 2.36\sqrt{S}E_{ph}\sqrt{\coth\left(\frac{E_{ph}}{2k_B T}\right)} \quad (2)$$

where the E_{ph} is the effective phonon energy, k_B is the Boltzmann constant, and T is temperature. For $Cs_5Cu_3Cl_6I_2$ NCs, S is calculated as 25.0 (Figure S12, Supporting Information), and this is larger than the value reported for single crystal ($S = 16$),[64] this can be assumed to be an effect caused by the size of the crystal being reduced to the nanoscale according to the previous studies.[106] The increase in S value in $Cs_5Cu_3Cl_6I_2$ NCs means that the probability of STEs formation has increased compared to their bulk counterparts, which led to near-unity PLQY of NCs. An interesting aspect is that there is an appropriate S range to promote luminescence at the STEs. In the case of a large S, such as $Cs_3Bi_2I_9$ (S = 79.5) and $Cs_3Sb_2I_9$ (S = 42.7), the excited state energy would be dissipated by phonons, resulting in low PLQY.[107–109] The increase in PLQY according to the increase in S within the appropriate range observed in $Cs_5Cu_3Cl_6I_2$ NCs is similar with the result in previous study that observed the change in PLQY according to the change in the S of $C_5N_2H_{16}Pb_2Br_6$.[110] In order to clearly demonstrate the superior thermal stability of the $Cs_5Cu_3Cl_6I_2$ NCs, we synthesized quantum-confined $CsPbBr_3$ NCs, which currently constitute the most attractive semiconductor material, and compared its performance with that of the $Cs_5Cu_3Cl_6I_2$ NC material in a thermal cycling test (Figure 4c). The PL of $CsPbBr_3$, which initially had a QY of 100% at 25 °C, deteriorated and its intensity was less than 10% at 100 °C. As the cycle was repeated, the PL intensity at room temperature also decreased significantly, and a new PL peak was observed at 520 nm owing to particle aggregation (Figure S13, Supporting Information). However, for $Cs_5Cu_3Cl_6I_2$, the PL intensity was maintained—at 100 °C—at >90% of its original value at 0 °C, and at room temperature the original PL intensity was recovered. This behavior did not change, even after four heating–cooling cycles over several

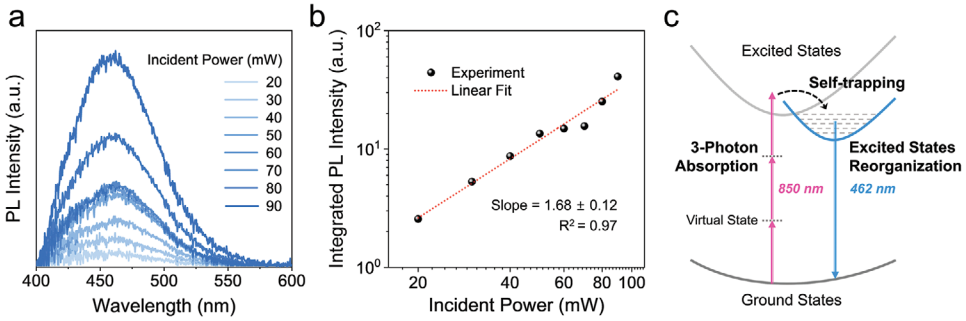

Figure 5. Nonlinear optical response of $Cs_5Cu_3Cl_6I_2$ NCs. a) Variation of 3PA-induced PL spectrum with incident femtosecond laser excitation power (λ_{ex} = 850 nm). b) Integrated PL intensity as a function of incident power in double logarithmic scale. c) Schematic representation of degenerate 3PA-induced PL.

hours, showing that the non-toxic $Cs_5Cu_3Cl_6I_2$ NC material is highly stable and can be used as a replacement for toxic Pb-based metal halides. Figure 4d shows a comparison of the XRD patterns acquired before and after thermal cycling; the high structural stability of the material, as evidenced by the absence of peak changes (i.e., peak shifts or the generation of new peaks), is apparent.

In contrast to their excellent optical properties and stability, the practical applicability of the synthesized $Cs_5Cu_3Cl_6I_2$ NCs is limited due to their relatively small absorption range in the UV region (λ_{abs} < 300 nm). To identify potential applications based on visible-to-NIR range optical excitation, we examined the nonlinear optical properties of the material, including its multiphoton absorption (MPA) capacity. The experimental setup used to investigate the MPA-induced PL of the $Cs_5Cu_3Cl_6I_2$ NCs with femtosecond laser excitation is presented schematically in Figure S14, Supporting Information. The absorption and PLE spectra of $Cs_5Cu_3Cl_6I_2$ include a very short-wavelength band with a peak at ≈285 nm. Under laser excitation at 850 nm (≈3 × 285 nm), a bright, highly focused blue emission signal, induced by degenerate three-photon absorption (3PA), was observed (Figure S15, Supporting Information). Unlike single-photon-induced PL, which is emitted over the entire laser beam path within a sample, the nonlinear nature of MPA-induced excitation means that emission occurs only at the focus of the excitation laser because the simultaneous absorption of multiple photons is most probable in this small volume of the sample.[111] To further clarify these results, we observed the change in integrated PL intensity according to the displacement of the Z position at the focal point (Z = 0). It was demonstrated that 3PA-induced PL steeply diminished as the sample moved away from the focal point (Figure S16, Supporting Information).

Figure 5 illustrates the 3PA-induced PL characteristics (Figure 5a) and underlying photophysics of the $Cs_5Cu_3Cl_6I_2$ NCs. The slope of the double logarithmic plot in Figure 5b (1.68 ± 0.12) reveals that the PL intensity increases nonlinearly with the incident excitation laser power. It is noteworthy that the slope is significantly smaller than 3, the value that would be expected for a typical 3PA-induced emission.[112,113] We speculate that this reduced number of photons (i.e., significantly <3) is sufficient to induce the PL emission because it mainly occurs from a self-trapped state of the $Cs_5Cu_3Cl_6I_2$ NCs. Figure 5c schematically illustrates this 3PA-induced PL process in the $Cs_5Cu_3Cl_6I_2$ NCs. The MPA characteristics of the $Cs_5Cu_3Cl_6I_2$ NCs, combined with their excellent luminescence properties and thermal stability, should further expand the application potential of the materials in the field of optoelectronics.

3. Conclusion

The need to improve the luminescence efficiency and stability of blue-emitting semiconductor nanomaterials is emerging, and Cu-based metal halides have been proposed to overcome the limitations of such existing nanomaterials. We focused on the Cu halide compound $Cs_5Cu_3Cl_6I_2$ and developed an optimized protocol to synthesize uniform NCs with superior PLQY. Through precise control of the synthesis parameters, we demonstrated a diverse range of effects for the material properties, from inducing anisotropic growth to tuning the energy of self-trapped states. The excellent thermal stability and nonlinear optical properties of the synthesized $Cs_5Cu_3Cl_6I_2$ NCs underline the significance of the STE-mediated luminescence mechanism, and highlight the potential of the new nanomaterial in various optoelectronic device applications. These findings provide insights into the colloidal synthesis of $Cs_5Cu_3Cl_6I_2$ NCs and hence should also act as a foundation for further advances in this field.

4. Experimental Section

Materials: Cesium carbonate (Cs_2CO_3, 99.9%), copper(I) acetate ($Cu(C_2H_3O_2)$, 99.7%), indium chloride ($InCl_3$, 99.999%), oleic acid (OAc, 90%), oleylamine (OAm, 70%), hydroiodic acid (HI, 57%), 1-octadecene (ODE, 90%), and *n*-hexane (anhydrous, 95%) were purchased from Sigma-Aldrich. All chemicals were used as received.

Synthesis of Cs-Oleate (Cs(OAc)) Solution: Cs_2CO_3 (0.408 g, 1.25 mmol), OAc (2 mL), and ODE (5 mL) were placed in a 50 mL three-neck round-bottom flask. The flask was slowly heated to 120 °C with degassing. After degassing the solution for 1 h at 120 °C, the flask was maintained at this temperature for 1 h in the Ar atmosphere.

Synthesis of Oleylammonium Iodide (OAm-I) Solution: OAm (30 mL) was added to a 100 mL three-neck round-bottom flask. After slowly injecting HI (4.5 mL) into the OAm, the temperature was raised to 80 °C and the mixture was allowed to react for 2 h. Then, the solution was degassed for 1 h to completely remove water. The resultant OAm-I solution was transferred to a vial and stored in an Ar-filled glove box.

Synthesis of $Cs_5Cu_3Cl_6I_2$ NCs (CCH-1) Solution: $Cu(C_2H_3O_2)$ (0.0368 g, 0.3 mmol), $InCl_3$ (0.0445 g, 0.2 mmol), the prepared OAm-I solution (0.2 mL), OAc (1.0 mL), OAm (1.2 mL), and ODE (8 mL) were loaded into

a 50 mL three-neck round-bottom flask. The flask was slowly heated to 120 °C with degassing and maintained at that temperature for 1 h. After purging with Ar, the solution was heated to 150 °C and allowed to react for 5 min. The solution was cooled to 80 °C and then Cs(OAc) solution (2 mL) was rapidly injected. After being allowed to react for 5 min with vigorous stirring, the solution was cooled to room temperature using an ice-water bath. The product solution was then centrifuged at 7830 rpm for 10 min. The supernatant was decanted and the precipitates were redispersed in *n*-hexane (10 mL). Next, the solution was centrifuged once again at 7830 rpm for 5 min, and the supernatant ($Cs_5Cu_3Cl_6I_2$ NCs solution) was taken. To synthesize CCH-2, the amounts of $InCl_3$ and the OAm-I solution were adjusted to 0.0511 g and 0.12 mL, respectively, and the reaction was carried out at 140 °C.

General Characterization: Absorption spectra were recorded using a Shimadzu UV-1800 UV–Vis spectrophotometer, and PL spectra were acquired using an Agilent Cary Eclipse fluorescence spectrophotometer. Absolute PLQYs were obtained from measurements acquired using a Hamamatsu C11347-11 spectrometer with an integrating sphere system. The inner wall of the integrating sphere was coated with a layer of PTFE which is highly reflective in the UV spectral range down to 200 nm. The NCs in hexane solution was prepared in a quartz cell, and the spectrum was collected at room temperature using 150 W xenon light source (excitation wavelength: 290 nm). TRPL measurements were acquired using an Edinburgh FS-5 fluorescence spectrometer in multi-channel scaling mode. The thermal quenching characteristics during heating were observed via fluorescence spectrometry (Hitachi F-7000 with integrated heater, temperature controller, and thermal sensor). TEM images were obtained using a Tecnai G2 F20 microscope (Ted Pella Inc.) with an acceleration voltage of 200 kV and gold grids. The $Cs_5Cu_3Cl_6I_2$ microcrystals were also observed using field-emission scanning electron microscopy (FE-SEM, Hitachi, SU8220). XRD analysis was carried out using a Bruker D2 Phaser X-ray diffractometer. XPS was performed using a Thermo Scientific K-Alpha system. Thin films of $Cs_5Cu_3Cl_{8-x}I_x$ NCs were prepared on glass substrates via spin-coating (2000 rpm).

Computational Details: DFT calculations were performed using the Vienna ab initio simulation package (VASP)[114,115] with the projector-augmented-wave (PAW) method.[116] The generalized gradient approximation (GGA) with the Perdew–Burke–Ernzerhof (PBE) functional was adopted to describe the electron exchange–correlation potential.[117] Electronic wave functions were expanded in a plane-wave basis set with a kinetic energy cutoff of 500 eV. The Brillouin zone was integrated with a gamma-centered $1 \times 3 \times 2$ *k*-point grid for geometry optimization and $3 \times 5 \times 4$ *k*-point grid for electronic structure calculations. The convergence criterion for the self-consistent field calculation was set to 1×10^{-6} eV. The lattice parameters and atomic positions were fully relaxed until the Hellmann–Feynman forces were less than 0.01 eV $Å^{-1}$.

MPA-Induced PL Measurements: An amplified ytterbium-based laser system (Pharos SP-06-600-PP, Light Conversion), which produces infrared pulses (6 W) centered at 1030 nm with a repetition rate of 200 kHz and a pulse width of 170 fs, was utilized to perform MPA experiments. The output beam was directed toward an optical parametric amplifier (OPA; Orpheus, Light Conversion) to generate a pump pulse at 850 nm for excitation. The resulting pump pulse passed through an 830-nm cut-on filter (FSQ-RG830, Newport), which removed residual second harmonic pulses from the optical parametric amplifier (OPA) output beam, and was tightly focused (FWHM = 0.3 mm) on the interior of a 3-mm transparent cuvette. The upconverted luminescence from the sample was collected normal to the excitation beam. This signal was then collimated and focused on a spectrophotometer (USB2000+, Ocean Optics). The power of the excitation beam was adjusted in the range of 20–90 mW using a rotatable neutral density filter. All the luminescence spectra were obtained under ambient conditions.

Supporting Information

Supporting Information is available from the Wiley Online Library or from the author.

Acknowledgements

C.J. and K.K. contributed equally to this work. This work was supported by grants funded by the Korean government (MSIT) from the National Research Foundation of Korea (NRF) (NRF-2021M3H4A3A01062963) and the Institute of Information & communications Technology Planning & evaluation (IITP) (No. 20210010330012002). This work was also supported by "the Research Project Funded by U-K Brand" (1.220033.01 and 1.220026.01) of UNIST.

Conflict of Interest

The authors declare no conflict of interest.

Data Availability Statement

The data that support the findings of this study are available in the supplementary material of this article.

Keywords

blue-emitting semiconductors, $Cs_5Cu_3Cl_6I_2$, metal halides, multiphoton absorption, Pb-free, self-trapped excitons, thermal stability

Received: October 29, 2022
Revised: December 19, 2022
Published online:

[1] Z. Guo, J. Li, R. Pan, J. Cheng, R. Chen, T. He, *Nanoscale* **2020**, *12*, 15560.
[2] Z. Xiao, Z. Song, Y. Yan, *Adv. Mater.* **2019**, *31*, 1803792.
[3] A. Jain, O. Voznyy, E. H. Sargent, *J. Phys. Chem. C* **2017**, *121*, 7183.
[4] J. S. Manser, J. A. Christians, P. V. Kamat, *Chem. Rev.* **2016**, *116*, 12956.
[5] H.-P. Wang, S. Li, X. Liu, Z. Shi, X. Fang, J.-H. He, *Adv. Mater.* **2021**, *33*, 2003309.
[6] W. Zhang, G. E. Eperon, H. J. Snaith, *Nat. Energy* **2016**, *1*, 16048.
[7] X.-K. Liu, W. Xu, S. Bai, Y. Jin, J. Wang, R. H. Friend, F. Gao, *Nat. Mater.* **2021**, *20*, 10.
[8] X. Wang, T. Li, B. Xing, M. Faizan, K. Biswas, L. Zhang, *J. Phys. Chem. Lett.* **2021**, *12*, 10532.
[9] F. Zhang, Z. Ma, Z. Shi, X. Chen, D. Wu, X. Li, C. Shan, *Energy Mater. Adv.* **2021**, *2021*, 38.
[10] W. Xiang, S. Liu, W. Tress, *Energy Environ. Sci.* **2021**, *14*, 2090.
[11] S. Zhao, W. Cai, H. Wang, Z. Zang, J. Chen, *Small Methods* **2021**, *5*, 2001308.
[12] F. Zhang, H. Zhong, C. Chen, X.-g. Wu, X. Hu, H. Huang, J. Han, B. Zou, Y. Dong, *ACS Nano* **2015**, *9*, 4533.
[13] L. Protesescu, S. Yakunin, S. Kumar, J. Bär, F. Bertolotti, N. Masciocchi, A. Guagliardi, M. Grotevent, I. Shorubalko, M. I. Bodnarchuk, C.-J. Shih, M. V. Kovalenko, *ACS Nano* **2017**, *11*, 3119.
[14] S. Seth, A. Samanta, *Sci. Rep.* **2016**, *6*, 37693.
[15] A. Pan, B. He, X. Fan, Z. Liu, J. J. Urban, A. P. Alivisatos, L. He, Y. Liu, *ACS Nano* **2016**, *10*, 7943.
[16] W. J. Mir, A. Alamoudi, J. Yin, K. E. Yorov, P. Maity, R. Naphade, B. Shao, J. Wang, M. N. Lintangpradipto, S. Nematulloev, A.-H. Emwas, A. Genovese, O. F. Mohammed, O. M. Bakr, *J. Am. Chem. Soc.* **2022**, *144*, 13302.

[17] S. Sun, D. Yuan, Y. Xu, A. Wang, Z. Deng, *ACS Nano* **2016**, *10*, 3648.
[18] L. Protesescu, S. Yakunin, M. I. Bodnarchuk, F. Krieg, R. Caputo, C. H. Hendon, R. X. Yang, A. Walsh, M. V. Kovalenko, *Nano Lett.* **2015**, *15*, 3692.
[19] D. Amgar, A. Stern, D. Rotem, D. Porath, L. Etgar, *Nano Lett.* **2017**, *17*, 1007.
[20] D. Yan, T. Shi, Z. Zang, T. Zhou, Z. Liu, Z. Zhang, J. Du, Y. Leng, X. Tang, *Small* **2019**, *15*, 1901173.
[21] W. Chen, J. Hao, W. Hu, Z. Zang, X. Tang, L. Fang, T. Niu, M. Zhou, *Small* **2017**, *13*, 1604085.
[22] L. Meng, J. You, Y. Yang, *Nat. Commun.* **2018**, *9*, 5265.
[23] Y. Zhou, Y. Zhao, *Energy Environ. Sci.* **2019**, *12*, 1495.
[24] M. Ren, X. Qian, Y. Chen, T. Wang, Y. Zhao, *J. Hazard. Mater.* **2022**, *426*, 127848.
[25] Y. Takahashi, R. Obara, Z.-Z. Lin, Y. Takahashi, T. Naito, T. Inabe, S. Ishibashi, K. Terakura, *Dalton Trans.* **2011**, *40*, 5563.
[26] Y. Takahashi, H. Hasegawa, Y. Takahashi, T. Inabe, *J. Solid State Chem.* **2013**, *205*, 39.
[27] P. Xu, S. Chen, H.-J. Xiang, X.-G. Gong, S.-H. Wei, *Chem. Mater.* **2014**, *26*, 6068.
[28] X. Wu, W. Song, Q. Li, X. Zhao, D. He, Z. Quan, *Chem. - Asian J.* **2018**, *13*, 1654.
[29] E. T. McClure, M. R. Ball, W. Windl, P. M. Woodward, *Chem. Mater.* **2016**, *28*, 1348.
[30] G. Volonakis, A. A. Haghighirad, R. L. Milot, W. H. Sio, M. R. Filip, B. Wenger, M. B. Johnston, L. M. Herz, H. J. Snaith, F. Giustino, *J. Phys. Chem. Lett.* **2017**, *8*, 772.
[31] M. R. Filip, X. Liu, A. Miglio, G. Hautier, F. Giustino, *J. Phys. Chem. C* **2018**, *122*, 158.
[32] F. Wei, Z. Deng, S. Sun, F. Zhang, D. M. Evans, G. Kieslich, S. Tominaka, M. A. Carpenter, J. Zhang, P. D. Bristowe, A. K. Cheetham, *Chem. Mater.* **2017**, *29*, 1089.
[33] T. Jun, K. Sim, S. Iimura, M. Sasase, H. Kamioka, J. Kim, H. Hosono, *Adv. Mater.* **2018**, *30*, 1804547.
[34] Z. Luo, Q. Li, L. Zhang, X. Wu, L. Tan, C. Zou, Y. Liu, Z. Quan, *Small* **2020**, *16*, 1905226.
[35] D. Yuan, *ACS Appl. Mater. Interfaces* **2020**, *12*, 38333.
[36] R. Lin, Q. Guo, Q. Zhu, Y. Zhu, W. Zheng, F. Huang, *Adv. Mater.* **2019**, *31*, 1905079.
[37] Z. Li, Z. Li, Z. Shi, X. Fang, *Adv. Funct. Mater.* **2020**, *30*, 2002634.
[38] X. Huang, Q. Sun, B. Devakumar, *Mater. Today Chem.* **2020**, *17*, 100288.
[39] S. Zhao, C. Chen, W. Cai, R. Li, H. Li, S. Jiang, M. Liu, Z. Zang, *Adv. Opt. Mater.* **2021**, *9*, 2100307.
[40] B. Wang, Y. Tang, X. Yang, W. Cai, R. Li, W. Ma, S. Zhao, C. Chen, Z. Zang, *Nano Mater. Sci.* **2022**, https://doi.org/10.1016/j.nanoms.2022.03.003.
[41] B. Wang, C. Chen, X. Yang, W. Cai, S. Zhao, R. Li, W. Ma, J. Chen, Z. Zang, *EcoMat* **2022**, *4*, e12184.
[42] Y. Zhang, Y. He, Z. Tang, W. Yu, Z. Zhang, Z. Chen, L. Xiao, J.-j. Shi, S. Wang, B. Qu, *Small* **2022**, *18*, 2107161.
[43] L. Lian, M. Zheng, P. Zhang, Z. Zheng, K. Du, W. Lei, J. Gao, G. Niu, D. Zhang, T. Zhai, S. Jin, J. Tang, X. Zhang, J. Zhang, *Chem. Mater.* **2020**, *32*, 3462.
[44] L. Wang, Z. Shi, Z. Ma, D. Yang, F. Zhang, X. Ji, M. Wang, X. Chen, G. Na, S. Chen, D. Wu, Y. Zhang, X. Li, L. Zhang, C. Shan, *Nano Lett.* **2020**, *20*, 3568.
[45] Z. Ma, Z. Shi, C. Qin, M. Cui, D. Yang, X. Wang, L. Wang, X. Ji, X. Chen, J. Sun, D. Wu, Y. Zhang, X. J. Li, L. Zhang, C. Shan, *ACS Nano* **2020**, *14*, 4475.
[46] X. Zhao, G. Niu, J. Zhu, B. Yang, J.-H. Yuan, S. Li, W. Gao, Q. Hu, L. Yin, K.-H. Xue, E. Lifshitz, X. Miao, J. Tang, *J. Phys. Chem. Lett.* **2020**, *11*, 1873.
[47] R. Roccanova, A. Yangui, G. Seo, T. D. Creason, Y. Wu, D. Y. Kim, M.-H. Du, B. Saparov, *ACS Mater. Lett.* **2019**, *1*, 459.
[48] P. Cheng, L. Sun, L. Feng, S. Yang, Y. Yang, D. Zheng, Y. Zhao, Y. Sang, R. Zhang, D. Wei, W. Deng, K. Han, *Angew. Chem., Int. Ed.* **2019**, *58*, 16087.
[49] R. Kentsch, M. Morgenroth, M. Scholz, K. Xu, J. S. auf der Günne, T. Lenzer, K. Oum, *J. Phys. Chem. Lett.* **2020**, *11*, 4286.
[50] L. Lian, M. Zheng, W. Zhang, L. Yin, X. Du, P. Zhang, X. Zhang, J. Gao, D. Zhang, L. Gao, G. Niu, H. Song, R. Chen, X. Lan, J. Tang, J. Zhang, *Adv. Sci.* **2020**, *7*, 2000195.
[51] F. Zeng, Y. Guo, W. Hu, Y. Tan, X. Zhang, J. Yang, Q. Lin, Y. Peng, X. Tang, Z. Liu, Z. Yao, J. Du, *J. Lumin.* **2020**, *223*, 117178.
[52] L. Xie, B. Chen, F. Zhang, Z. Zhao, X. Wang, L. Shi, Y. Liu, L. Huang, R. Liu, B. Zou, Y. Wang, *Photonics Res.* **2020**, *8*, 768.
[53] R. Roccanova, A. Yangui, H. Nhalil, H. Shi, M.-H. Du, B. Saparov, *ACS Appl. Electron. Mater.* **2019**, *1*, 269.
[54] P. Du, L. Luo, W. Cheng, *J. Am. Ceram. Soc.* **2020**, *103*, 1149.
[55] F. Zeng, Y. Guo, W. Hu, Y. Tan, X. Zhang, J. Feng, X. Tang, *ACS Appl. Mater. Interfaces* **2020**, *12*, 23094.
[56] Q. Li, Z. Chen, B. Yang, L. Tan, B. Xu, J. Han, Y. Zhao, J. Tang, Z. Quan, *J. Am. Chem. Soc.* **2020**, *142*, 1786.
[57] S. Fang, Y. Wang, H. Li, F. Fang, K. Jiang, Z. Liu, H. Li, Y. Shi, *J. Mater. Chem. C* **2020**, *8*, 4895.
[58] Y. Li, P. Vashishtha, Z. Zhou, Z. Li, S. B. Shivarudraiah, C. Ma, J. Liu, K. S. Wong, H. Su, J. E. Halpert, *Chem. Mater.* **2020**, *32*, 5515.
[59] Y. Li, Z. Shi, L. Wang, Y. Chen, W. Liang, D. Wu, X. Li, Y. Zhang, C. Shan, X. Fang, *Mater. Horiz.* **2020**, *7*, 1613.
[60] P. Sebastia-Luna, J. Navarro-Alapont, M. Sessolo, F. Palazon, H. J. Bolink, *Chem. Mater.* **2019**, *31*, 10205.
[61] X. Zheng, J. Huang, Y. Liu, T. Wang, S. Han, Z. Wang, B. Teng, S. Ji, *Adv. Photonics Res.* **2022**, *3*, 2100289.
[62] F. Zhang, Z. Zhao, B. Chen, H. Zheng, L. Huang, Y. Liu, Y. Wang, A. L. Rogach, *Adv. Opt. Mater.* **2020**, *8*, 1901723.
[63] B. Wang, Z. Jia, X. Yang, S. Lu, J. Zhao, Z. Sun, Q. Qian, Q. Lin, Z. Zang, *Chem. Commun.* **2022**, *58*, 13206.
[64] J. Li, T. Inoshita, T. Ying, A. Ooishi, J. Kim, H. Hosono, *Adv. Mater.* **2020**, *32*, 2002945.
[65] J. Duan, J. Xi, B. Jiao, J. Dai, Y. Zu, Z. Wu, *J. Mater. Chem. C* **2022**, *10*, 11323.
[66] Q. Guo, X. Zhao, B. Song, J. Luo, J. Tang, *Adv. Mater.* **2022**, *34*, 2201008.
[67] B. Zhang, X. Wu, S. Zhou, G. Liang, Q. Hu, *Front. Optoelectron.* **2021**, *14*, 459.
[68] S. Li, J. Luo, J. Liu, J. Tang, *J. Phys. Chem. Lett.* **2019**, *10*, 1999.
[69] J. Li, H. Wang, D. Li, *Front. Optoelectron.* **2020**, *13*, 225.
[70] Z. Xu, X. Jiang, H.-p. Cai, K. Chen, X. Yao, Y. Feng, *J. Phys. Chem. Lett.* **2021**, *12*, 10472.
[71] B. O. Dabbousi, J. Rodriguez-Viejo, F. V. Mikulec, J. R. Heine, H. Mattoussi, R. Ober, K. F. Jensen, M. G. Bawendi, *J. Phys. Chem. B* **1997**, *101*, 9463.
[72] S. Nizamoglu, H. V. Demir, *Opt. Express* **2008**, *16*, 3515.
[73] A. Mews, A. Kadavanich, U. Banin, A. Alivisatos, *Phys. Rev. B* **1996**, *53*, R13242.
[74] M. A. Hines, P. Guyot-Sionnest, *J. Phys. Chem.* **1996**, *100*, 468.
[75] S. Feldmann, M. K. Gangishetty, I. Bravić, T. Neumann, B. Peng, T. Winkler, R. H. Friend, B. Monserrat, D. N. Congreve, F. Deschler, *J. Am. Chem. Soc.* **2021**, *143*, 8647.
[76] J. Butkus, P. Vashishtha, K. Chen, J. K. Gallaher, S. K. K. Prasad, D. Z. Metin, G. Laufersky, N. Gaston, J. E. Halpert, J. M. Hodgkiss, *Chem. Mater.* **2017**, *29*, 3644.
[77] G. Ghosh, B. Jana, S. Sain, A. Ghosh, A. Patra, *Phys. Chem. Chem. Phys.* **2019**, *21*, 19318.
[78] K. Marjit, G. Ghosh, S. Ghosh, S. Sain, A. Ghosh, A. Patra, *J. Phys. Chem. C* **2021**, *125*, 12214.
[79] X. Kong, Y. Wu, F. Xu, S. Yang, B. Cao, *Phys. Status Solidi RRL* **2021**, *15*, 2100134.

[80] A. Di Giacomo, C. Rodà, A. H. Khan, I. Moreels, *Chem. Mater.* **2020**, *32*, 9260.
[81] J. Cho, Y. K. Jung, J.-K. Lee, H.-S. Jung, *Langmuir* **2017**, *33*, 3711.
[82] S.-H. Lee, S.-W. Song, S.-Y. Yoon, D.-Y. Jo, S.-K. Kim, H.-M. Kim, Y. Kim, S. M. Park, H. Yang, *Chem. Eng. J.* **2022**, *429*, 132464.
[83] C.-Y. Han, S.-H. Lee, S.-W. Song, S.-Y. Yoon, J.-H. Jo, D.-Y. Jo, H.-M. Kim, B.-J. Lee, H.-S. Kim, H. Yang, *ACS Energy Lett.* **2020**, *5*, 1568.
[84] S.-W. Song, S.-H. Lee, D.-Y. Jo, S.-Y. Yoon, H.-M. Kim, Y. Kim, J.-N. Han, Y.-J. Lee, Y. R. Do, H. Yang, *Adv. Opt. Mater.* **2022**, *10*, 2101767.
[85] E.-P. Jang, C.-Y. Han, S.-W. Lim, J.-H. Jo, D.-Y. Jo, S.-H. Lee, S.-Y. Yoon, H. Yang, *ACS Appl. Mater. Interfaces* **2019**, *11*, 46062.
[86] R. K. Behera, S. Das Adhikari, S. K. Dutta, A. Dutta, N. Pradhan, *J. Phys. Chem. Lett.* **2018**, *9*, 6884.
[87] G. Pan, X. Bai, W. Xu, X. Chen, Y. Zhai, J. Zhu, H. Shao, N. Ding, L. Xu, B. Dong, Y. Mao, H. Song, *ACS Appl. Mater. Interfaces* **2020**, *12*, 14195.
[88] C. Wang, D. Han, J. Wang, Y. Yang, X. Liu, S. Huang, X. Zhang, S. Chang, K. Wu, H. Zhong, *Nat. Commun.* **2020**, *11*, 6428.
[89] Y. Wu, C. Wei, X. Li, Y. Li, S. Qiu, W. Shen, B. Cai, Z. Sun, D. Yang, Z. Deng, H. Zeng, *ACS Energy Lett.* **2018**, *3*, 2030.
[90] J. Leng, T. Wang, X. Zhao, E. W. Y. Ong, B. Zhu, J. D. A. Ng, Y.-C. Wong, K. H. Khoo, K. Tamada, Z.-K. Tan, *J. Phys. Chem. Lett.* **2020**, *11*, 2036.
[91] G. Genchi, M. S. Sinicropi, G. Lauria, A. Carocci, A. Catalano, *Int. J. Environ. Res. Public Health* **2020**, *17*, 3782.
[92] A. L. Wani, A. Ara, J. A. Usmani, *Interdiscip. Toxicol.* **2015**, *8*, 55.
[93] M. W. Ashraf, S. I. Haider, A. R. Solangi, A. F. Memon, *Phys. Sci. Rev.* **2022**, *0*, https://doi.org/10.1515/psr-2021-0112.
[94] C. Shen, Y. Zhu, H. Tao, J. Li, J. Zou, L. Wang, J. Liang, X. Xiao, X. Xu, G. Xu, *ACS Appl. Nano Mater.* **2022**, *5*, 2801.
[95] H. Zhang, X. Ma, Q. Lin, Z. Zeng, H. Wang, L. S. Li, H. Shen, Y. Jia, Z. Du, *J. Phys. Chem. Lett.* **2020**, *11*, 960.
[96] W. Zhang, S. Ding, W. Zhuang, D. Wu, P. Liu, X. Qu, H. Liu, H. Yang, Z. Wu, K. Wang, X. W. Sun, *Adv. Funct. Mater.* **2020**, *30*, 2005303.
[97] W. Lee, C. Lee, B. Kim, Y. Choi, H. Chae, *Nanomaterials* **2020**, *10*, 2171.
[98] D. Zhang, S. W. Eaton, Y. Yu, L. Dou, P. Yang, *J. Am. Chem. Soc.* **2015**, *137*, 9230.
[99] D. Zhang, Y. Yang, Y. Bekenstein, Y. Yu, N. A. Gibson, A. B. Wong, S. W. Eaton, N. Kornienko, Q. Kong, M. Lai, A. P. Alivisatos, S. R. Leone, P. Yang, *J. Am. Chem. Soc.* **2016**, *138*, 7236.
[100] S. Aharon, L. Etgar, *Nano Lett.* **2016**, *16*, 3230.
[101] Y. Dong, T. Qiao, D. Kim, D. Parobek, D. Rossi, D. H. Son, *Nano Lett.* **2018**, *18*, 3716.
[102] G. Lefèvre, A. Walcarius, J. J. Ehrhardt, J. Bessière, *Langmuir* **2000**, *16*, 4519.
[103] C. H. Chia, C. T. Yuan, J. T. Ku, S. L. Yang, W. C. Chou, J. Y. Juang, S. Y. Hsieh, K. C. Chiu, J. S. Hsu, S. Y. Jeng, *J. Lumin.* **2008**, *128*, 123.
[104] C.-H. Chia, W.-C. Fan, Y.-C. Lin, W.-C. Chou, *J. Lumin.* **2011**, *131*, 956.
[105] W. Stadler, D. M. Hofmann, H. C. Alt, T. Muschik, B. K. Meyer, E. Weigel, G. Müller-Vogt, M. Salk, E. Rupp, K. W. Benz, *Phys. Rev. B* **1995**, *51*, 10619.
[106] P. Nandakumar, C. Vijayan, *J. Appl. Phys.* **2002**, *91*, 1509.
[107] J. Luo, X. Wang, S. Li, J. Liu, Y. Guo, G. Niu, L. Yao, Y. Fu, L. Gao, Q. Dong, C. Zhao, M. Leng, F. Ma, W. Liang, L. Wang, S. Jin, J. Han, L. Zhang, J. Etheridge, J. Wang, Y. Yan, E. H. Sargent, J. Tang, *Nature* **2018**, *563*, 541.
[108] H. Peng, B. Zou, *J. Phys. Chem. Lett.* **2022**, *13*, 1752.
[109] J. Jin, Y. Peng, Y. Xu, K. Han, A. Zhang, X.-B. Yang, Z. Xia, *Chem. Mater.* **2022**, *34*, 5717.
[110] H. Luo, S. Guo, Y. Zhang, K. Bu, H. Lin, Y. Wang, Y. Yin, D. Zhang, S. Jin, W. Zhang, W. Yang, B. Ma, X. Lu, *Adv. Sci.* **2021**, *8*, 2100786.
[111] G. C. R. Ellis-Davies, *Front. Synaptic Neurosci.* **2019**, *10*, https://doi.org/10.3389/fnsyn.201800048.
[112] M. Wang, M. Kim, F. Xia, C. Xu, *Biomed. Opt. Express* **2019**, *10*, 1905.
[113] Z. Guo, J. Li, Y. Gao, J. Cheng, W. Zhang, R. Pan, R. Chen, T. He, *J. Mater. Chem. C* **2020**, *8*, 16923.
[114] G. Kresse, J. Furthmüller, *Comput. Mater. Sci.* **1996**, *6*, 15.
[115] G. Kresse, J. Furthmüller, *Phys. Rev. B* **1996**, *54*, 11169.
[116] G. Kresse, D. Joubert, *Phys. Rev. B* **1999**, *59*, 1758.
[117] J. P. Perdew, K. Burke, M. Ernzerhof, *Phys. Rev. Lett.* **1996**, *77*, 3865.